On the microwave background anisotropy produced by big voids in open universes

M.J. Fullana [1], **J.V. Arnau** [2], **& D. Sáez** [1]

[1] Departament d'Astronomia i Astrofísica. Universitat de València.

46100 Burjassot (València), Spain.

[2] Departament de Matemàtica Aplicada. Universitat de València.

46100 Burjassot (València), Spain.

e-mail: DIEGO.SAEZ@UV.ES

Abstract

The Tolman-Bondi solution of the Einstein equations is used in order to model the time evolution of the void observed in Boötes. The present density contrast of the central region (~ -0.75) and its radius ($\sim 30h^{-1}\ Mpc$) are fixed, while the density parameter of the Universe, the amplitude of the density contrast inside the void wall, the width of this wall and the distance from the void centre to the Local Group are appropriately varied. The microwave background anisotropy produced by Boötes-like voids is estimated for a significant set of locations. All the voids are placed far from the last scattering surface. It is shown that the anisotropy generated by these voids strongly depends on the density parameter, the wall structure and the void location. The Doppler dipole and quadrupole are subtracted and the residual anisotropy is calculated.

In the case of some isolated Boötes-like voids placed at redshifts between 1 and 10 in an open universe with density parameter $\Omega_0 = 0.2$, the residual anisotropy appears to be a few times 10^{-6} on scales of a few degrees. This anisotropy is about one order of magnitude greater than previous estimates corresponding to other cases. The anisotropy produced by a distribution of voids is qualitatively studied in the light of this result. Comparisons with previous estimates are discussed.

Key words: cosmic microwave background (12.03.1) – methods: numerical (03.13.4)

1 Introduction

Two methods have been used in order to estimate the anisotropies produced by the nonlinear voids of the galaxy distribution in *open universes*. One of these methods is based on the so-called *Swiss-Cheese* model (Rees & Sciama 1968). The original version of this model applies to the case of overdensities surrounded by underdensities, but suitable modifications lead to a model for underdensities surrounded by overdensities (Thompson & Vishniac 1987). Estimates of the anisotropies produced by Swiss-Cheese voids were obtained by Thompson & Vishniac (1987), and Martínez-González & Sanz (1990). The main elements of these spherical voids are: an absolute vacuum in the void core, a uniform overdense shell compensating the vacuum, and a general Friedmann-Robertson-Walker background outside this shell; hence, the density profile of the resulting structure is very particular, while the background is general and the compensation is exact. The second method is based on the Tolman-Bondi Solution (TBS) of the Einstein equations (Tolman 1934; Bondi 1947). A general assymptotic Friedmann-Robertson-Walker background and a general spherically symmetric energy density profile are compatible with this solution; such a general profile can be used in order to model both a partial vacuum in the void core and a sharped wall. Two different codes based on the TBS were built up by Panek (1992) and Arnau et al. (1993). Panek's code was used (Panek 1992) to estimate the anisotropy produced by voids with small compensating walls, while the code due to Arnau et al. was used (Arnau et al. 1993) in the case of voids without walls; here, the void walls are

modeled in some detail taking into account some observational data.

In *flat universes*, another powerful method is being used in order to estimate the anisotropy produced by nonlinear cosmological structures. This method does not require any symmetry, it is based on the potential approximation developed by Martínez-González, Sanz & Silk (1990), which applies beyond the linear regime. In the flat case, the method was applied by Anninos et al. (1991), Martínez-González, Sanz & Silk (1992, 1994), Tuluie & Laguna (1995) and Quilis, Ibáñez & Sáez (1995); these authors used various complementary techniques and conditions (N-body simulations, high resolution shock capturing methods and particular spectra and statistics).

Recently, Arnau, Fullana & Sáez (1994) proved that some Great Attractor-like structures –evolving in open universes ($\Omega_0 < 0.4$) and placed at redshifts between 2 and 30– produce anisotropies of the order of 10^{-5} on angular scales of a few degrees. These structures had a density contrast of the order of 1 when they influenced the microwave photons; hence, the resulting nonlinear gravitational anisotropies are produced in the mildly nonlinear regime. The following question arises: Are there void-like objects –suitable structures, locations and backgrounds– producing significant anisotropies as in the case of the Great Attractor-like objects studied by Arnau, Fullana & Sáez (1994)?. In the case of nonlinear structures (density contrasts $\delta > 0.1$) evolving in open universes, the TBS and the Swiss-Cheese model can be used in order to answer this question. The use of the TBS seems to be preferable because this solution involves appropriate density profiles.

In order to model void-like objects, some observational data must be taken into account. In the eighties, there has been a great deal of observations on the spatial distribution of galaxies; in these observations, some voids with walls have been detected (Kirshner et al. 1981, Davis et al. 1982, Vettolani et al. 1985, de Lapparent, Geller & Huchra 1986, Rood 1988, Dey, Strauss & Huchra 1990); among them, the Boötes Void (BV) seems to be the greatest one. This void was first described by Kirshner et al. (1981). From the data given by these authors and those due to de Lapparent, Geller & Huchra (1986) it follows that the void in Boötes is a big quasispherical region with a defect of galaxies; its centre is located at $\sim 150\ h^{-1}\ Mpc$ from the Local Group and its radius is $\sim 30\ h^{-1}\ Mpc$. This region only contains the 25% of the galaxies expected in the same volume of the background; hence, the energy density contrast of galaxies inside the void is ~ -0.75. Surrounding this region, there is an irregular shell having an excess of galaxies, in other words, there is an inhomogeneous sharped wall. Although the observations are not very accurate (Kirshner et al. 1981, de Lapparent, Geller & Huchra 1986), current data suggest that the amplitude of the density contrast of galaxies inside the wall is ~ 4 and the mean width of this wall is $\sim 5h^{-1}\ Mpc$.

The above observational data must be complemented with appropriate assumptions about the dark matter distribution. Since the nonlinear anisotropy produced by voids located far from the last scattering surface is a gravitational effect, this anisotropy is produced by the total energy density contrast $\frac{\Delta\rho}{\rho}$. This contrast can be

obtained from the observational value of the density contrast produced by galaxies $(\frac{\Delta\rho}{\rho})_{gal}$ and the value of the the so-called *linear bias parameter* b. This parameter is defined by the relation $(\frac{\Delta\rho}{\rho})_{gal} = b(\frac{\Delta\rho}{\rho})$. In this paper, it is assumed that luminous galaxies trace the mass distribution. This means that the parameter b is assumed to be unity and, consequently, the relative defects (excesses) of galaxies and dark matter are identical inside the void (wall). The case $b < 1$ has not either theoretical or observational support, it corresponds to a void (wall) with an amount of dark matter smaller (greater) than that of the case $b = 1$; by this reason, the anisotropy of the case $b < 1$ is expected to be greater than that estimated in the case $b = 1$. Similar arguments lead to the conclusion that, in the case $b > 1$, the anisotropies are smaller than those of the case $b = 1$. Since the condition $b = 1$ is used along the paper, we can state that our computations give upper limits to the anisotropy produced by Boötes-like objects, except in the unlikely case $b < 1$.

In this paper, the wall is described by two parameters, the amplitude, $(\frac{\Delta\rho}{\rho})_{max}$, of the total density contrast inside the wall and the distance, d_w, between the two points of the wall in which $\frac{\Delta\rho}{\rho}$ is the 20% of $(\frac{\Delta\rho}{\rho})_{max}$; the distance d_w is called the wall width. In the case $b = 1$, current data suggest that the value of $(\frac{\Delta\rho}{\rho})_{max}$ is ~ 4 and the wall width d_w is $\sim 5h^{-1}$ Mpc. It can be easily verified (see Section 2) that a wall having these features overcompensates the central underdensity described above. The mass excess of this wall is about two times the mass defect of the underdense region. This is not a model dependent conclusion, but a direct consequence of the observations. In

this task, the anisotropy produced by an isolated structure is estimated. The chosen overcompensated structure is formed by a void and all the matter surrounding it. According to the above observational evidences, overcompensated structures of this kind are present in the universe. As required by the cosmological principle, each of these structures should be compensated by other structures in large volumes containing various voids. In order to imagine this compensation, it is useful to take into account that the energy excess surrounding a certain underdensity is shared by the neighboring ones and, consequently, this excess also contributes to the compensation of other neighboring underdensities; in other words, only a part of this excess must compensate the central underdensity.

The anisotropy produced by a realistic distribution of irregular voids and walls cannot be calculated from the anisotropy produced by an isolated void with walls; nevertheless, if the chosen isolated structure produces large enough anisotropies and its spatial distribution is appropriate, the true distribution of voids could produce relevant effects; in this case, the information obtained from the study of isolated structures strongly motivates further researches based on suitable approaches. Since the effects of isolated voids with walls placed far from the last scattering surface are expected to be small, the greatest observed void, namely, the BV has been selected. Several BV realizations evolving in various backgrounds have been considered in order to do an exhaustive study of the anisotropies produced by isolated voids. Observational evidences are taken into account in order to select these realizations

and backgrounds.

Henceforth, a is the scale factor, t is the cosmological time, an overdot stands for a derivative with respect to t, H is the ratio $\dot{a}/a$, and Ω_0 is the density parameter. The subscripts D, 0 and B indicate that a quantity has been valued at decoupling, at present time and in the background, respectively; for instance, H_0 is the Hubble constant. If H_0 is given in units of $km\ s^{-1}\ Mpc^{-1}$, the parameter $h = H_0/100$ is the reduced dimensionless Hubble constant.

The plan of this paper is as follows: Several BV models compatible with current observations are defined in Section 2. The initial conditions –at decoupling– leading to these models are derived in Section 3. The anisotropies produced by the BV models of Section 2 are presented in Section 4; appropriate comparisons with previous computations are also given in this section. Finally, the main conclusions are summarized and discussed in Section 5.

2 BV models

A BV realization is defined by the present density contrast inside the void $(\frac{\Delta\rho}{\rho})_v$, the present radius of the underdense region R_v, the present amplitude of the density contrast inside the wall $(\frac{\Delta\rho}{\rho})_{max}$ and the present wall width d_w. Any present configuration of the void in Boötes is a BV realization. Each BV realization is the final state of an evolutionary process, which takes place in a certain Friedmann-Robertson-Walker Universe. Hereafter, a BV realization and a background define a BV model. Any

model describes the time evolution of the void in a certain background. This evolution leads to a present state (a realization). If the cosmological constant vanishes, h and Ω_0 are the free parameters of the background. The numerical codes need a fixed value of h; nevertheless, if the distances are given in units of h^{-1} Mpc, the final results do not depend on the chosen value of h; so, only the background parameter Ω_0 is a physically significant free parameter to be varied.

Six BV realizations have been selected to be considered in the next sections.

One of the chosen BV realizations corresponds to $(\frac{\Delta\rho}{\rho})_v \sim -1$, $R_v \sim 30h^{-1}$ Mpc, $(\frac{\Delta\rho}{\rho})_{max} \sim 2.5$ and $d_w \sim 2h^{-1}$ Mpc. This realization is only studied in the case $\Omega_0 = 1$. The resulting model is considered with the essential aim of testing our codes and comparing our results with previous ones (Panek 1992)

The remaining five BV realizations are obtained as follows:

The quantities $(\frac{\Delta\rho}{\rho})_v$ and R_v are fixed; their values are assumed to be ~ -0.75 and $30h^{-1}$ Mpc, respectively. The amplitude $(\frac{\Delta\rho}{\rho})_{max}$ is varied from 2 to 6, and the wall width d_w is varied from $3h^{-1}$ Mpc to $7h^{-1}$ Mpc. Taking into account that the values of these parameters suggested by the observations (de Lapparent, Geller & Huchra 1986) are $(\frac{\Delta\rho}{\rho})_{max} \sim 4$ and $d_w \sim 5h^{-1}$ Mpc, we proceed as follows: in a first step, the wall width $d_w = 5h^{-1}$ Mpc is fixed and the amplitudes 2, 4 and 6 are considered and, in a second step, the amplitude $(\frac{\Delta\rho}{\rho})_{max} = 4$ is fixed and the wall widths are assumed to be $3h^{-1}$ Mpc, $5h^{-1}$ Mpc and $7h^{-1}$ Mpc. Note that the realization $(\frac{\Delta\rho}{\rho})_{max} \sim 4$ and $d_w \sim 5h^{-1}$ Mpc is considered in each of the above steps. Hereafter, any of these

five realizations is identified by the values of the quantities $(\frac{\Delta\rho}{\rho})_{max}$ and d_w. Each of these realizations has been studied in several cases corresponding to Ω_0 values ranging from 0.2 to 1; nevertheless, for the sake of briefness, only some appropriate models corresponding to $\Omega_0 = 0.2$ and $\Omega_0 = 1$ are presented.

For each BV realization, the wall compensates the central underdensity at a certain distance from the void centre. This distance is called the compensation radius, R_c. Tables 1 and 2 (seventh column) show these radius for all the models considered in this paper. In the cases of the first and fourth rows of Table 1 and the second row of Table 2, the compensation occurs outside the wall, while in the remaining cases, it occurs inside the wall; for example, in the case $(\frac{\Delta\rho}{\rho})_{max} \sim 4$ and $d_w \sim 5h^{-1}\ Mpc$, the compensation radius is $R_c = 32.7h^{-1}\ Mpc$ and, consequently, the compensation of the central underdensity takes place near the wall centre; this means that about one-half of the wall compensates the central void, while the remaining of the wall must compensate other underdensities.

For a given Ω_0 value, the quantities defining any BV realization (present contrasts and distances) must be numerically obtained –after evolution– from appropriated initial conditions; the choice of the initial conditions corresponding to a given model (a BV realization evolving in a defined background) is now discussed.

3 Initial conditions

The main goal of this task is the estimation of the secondary gravitational anisotropies produced by big voids located far from the last scattering surface. Since the evolution of the microwave photons must be studied from the last scattering surface to our position in the Universe, the initial conditions for the void evolution are set at decoupling time (redshift $z_{dec} = 1000$).

The initial profiles of the total energy density and the peculiar velocity field fix the two arbitrary functions involved in the TBS (see Arnau et al. 1993); hence, these initial profiles fix the time evolution of the resulting void from decoupling to present time.

In this paper, the initial density profile is assumed to be

$$\rho = \rho_{_{BD}} \left[1 + \frac{\varepsilon_1}{1 + (R/R_{x1})^6} + \frac{\varepsilon_2}{1 + (R/R_{x2})^6} \right] \;, \tag{1}$$

where R is a radial coordinate and the conditions $\varepsilon_1 > 0, \varepsilon_2 < 0, |\varepsilon_1| < |\varepsilon_2|$ and $R_{x1} > R_{2x}$ are satisfied.

The initial peculiar velocity is

$$V_{_D} = -\frac{1}{3} H_{_D} R \left\langle \frac{\rho - \rho_{_{BD}}}{\rho_{_{BD}}} \right\rangle \Omega_{_D}^{0.6} \tag{2}$$

where the angular brackets denote a mean value from $R = 0$ to R.

Since the cosmological constant vanishes, the background parameters involved in Eqs. (1) and (2) can be written in terms of Ω_0 and h.

Only the choice of the profile (1) is arbitrary. The profile (2) is obtained from Eq. (1). It corresponds to vanishing nongrowing modes (Peebles 1980). The form of the initial density profile (1) has not any theoretical justification. This form only gives a certain parametrization of the initial conditions, this parametrization is expected to be suitable in order to describe voids with walls as a result of two facts: (1) for small values of R/R_{x2}, the quantities $(R/R_{x1})^6$ and $(R/R_{x2})^6$ become very small and ρ becomes quasiconstant; this means that the profile (1) describes a central underdensity with a density contrast $\sim \varepsilon_1 + \varepsilon_2 < 0$ and, (2) the central underdensity is initially surrounded by an overdensity, which is the origin of the present void wall. It has been verified that the exponent 6 is suitable in order to get the required amplitudes and wall widths at present time, but other exponents could be also tested.

A realization is defined by the quantities $(\frac{\Delta\rho}{\rho})_v$, R_v, $(\frac{\Delta\rho}{\rho})_{max}$ and d_w. The question is: which are the values of the parameters ε_1, ε_2, R_{x1} and R_{x2} leading to a given realization in a fixed background?.

For each Ω_0 value, a numerical code based on the TBS plus Eqs. (1) and (2) calculates the quantities $(\frac{\Delta\rho}{\rho})_v$, R_v, $(\frac{\Delta\rho}{\rho})_{max}$ and d_w from initial values of ε_1, ε_2, R_{x1} and R_{x2}; this means that the quantities defining a BV realization are not initial conditions for the numerical code, but quantities derived from it.

Given a BV model, the corresponding initial conditions are obtained as follows:

arbitrary values of ε_1, ε_2, R_{x1} and R_{x2} are assumed and the resulting values of $(\frac{\Delta\rho}{\rho})_v$, R_v, $(\frac{\Delta\rho}{\rho})_{max}$ and d_w are compared with those of the chosen model; if they are different, the parameters ε_1, ε_2, R_{x1} and R_{x2} are varied and the results are compared again. These calculations and comparisons are carried out by a numerical code based on the "gradient method" (as in Sáez, Arnau & Fullana 1993). This code modifies the initial values of the parameters ε_1, ε_2, R_{x1} and R_{x2} in such a way that the new parameters lead to a BV model better than the previous one. This code repeats the modification of the parameters until the resulting BV model is similar enough to the required one. This process requires nonlinear techniques because the final BV model is a nonlinear one (see Fig. 1); in other words, nonlinear methods are necessary as a result of our BV normalization, which is based on present nonlinear observational data.

Table 1 gives the initial values of the parameters ε_1, ε_2, R_{x1} and R_{x2} for each of the $\Omega_0 = 0.2$ models studied in this paper. Table 2 gives the same information for the $\Omega_0 = 1$ models. The present $\frac{\Delta\rho}{\rho}$ profiles corresponding to our BV models are shown in Fig. 1. For a given realization, the present energy density profiles of the models $\Omega_0 = 0.2$ and $\Omega_0 = 1$ are indistinguishable because the same values of $(\frac{\Delta\rho}{\rho})_v$, R_v, $(\frac{\Delta\rho}{\rho})_{max}$ and d_w have been chosen in both cases (see Tables 1 and 2).

It is well known that the TBS only applies before shell crossing. Hellaby and Lake (1985) gave the necessary and sufficient conditions for the presence of shell crossing; these conditions are satisfied in the cases studied in this paper; hence, the shell crossing is unavoidable. The time at which this phenomenon takes place is not

given by the Hellaby and Lake conditions; this time must be determined in each particular case. In the cases studied in this paper, it has been verified that the shell crossing does not take place before present time; hence, the TBS can be used in our computations.

4 Anisotropy

The initial conditions discussed in Sect. 3 define the space-time structure and, consequently, these conditions fix the differential equations of the photon trajectories. These differential equations must be integrated in order to estimate the anisotropy produced by a BV model; this integration is carried out by using the code due to Arnau et al. (1993) and Sáez, Arnau & Fullana (1993) plus the initial profiles (1) and (2).

The centre of the BV open models ($\Omega_0 = 0.2$) has been located at a significant set of distances from the observer, which correspond to redshifts between 0.052 ($\sim 150h^{-1}\ Mpc$) and 100 ($8360h^{-1}\ Mpc$); nevertheless, only the results corresponding to a few appropriate distances are displayed in the Figures. The centre of the BV flat model corresponding to the first row of Table 2 has been placed at the same redshifts, while the model used for comparisons with previous computations (second row of Table 2) has been only located at $100h^{-1}\ Mpc$ in order to facilitate these comparisons; hence, all the selected structures are located far from the last scattering surface and, consequently, they produce negligible temperature fluctuations and Doppler shifts on

this surface; in which, the temperature is assumed to be constant.

Our code (Arnau et al. 1993, Sáez, Arnau & Fullana 1993) numerically computes the temperature T of the microwave background as a function of the observation angle ψ; this is the angle formed by the line of sight and the line joining the observer and the inhomogeneity centre. The function $T(\psi)$ is then used to calculate the mean temperature $< T > = (1/2) \int_0^\pi T(\psi) \; sin\psi \; d\psi$ and the total temperature contrast $\delta_T(\psi) = [T(\psi) - < T >] \; / \; < T >$. In the expansion of δ_T in spherical harmonics, $\delta_T(\psi) = D \; cos\psi + Q \; (3cos^2 \; \psi - 1) + \textit{higher order multipoles}$, D and Q are the total dipole and quadrupole, respectively. The dipole D is assumed to be a Doppler effect appearing as a result of the present peculiar velocity of the observer produced by the Boötes-like object; in other words, any gravitational contribution to the dipole is neglected; thus the relativistic Doppler quadrupole is $D^2/3$. The total Doppler effect (dipole and quadrupole) produced by the peculiar motion of the observer is subtracted from $\delta_T(\psi)$ to obtain the residual anisotropy $\delta_R(\psi) = \delta_T(\psi) - D \; cos\psi - D^2/3 \; (3cos^2 \; \psi - 1)$; therefore, on account of the large distance separating the chosen voids from the last scattering surface, this anisotropy is a pure gravitational effect. The rigorous computation of this effect requires nonlinear techniques when the amplitude of the density contrast reaches values greater than ~ 0.1 in some region of the structure.

The residual anisotropies produced by the BV models of Sect. 2 –for appropriate locations– are now presented and discussed.

4.1 Open Universe, $\Omega_0 = 0.2$

The upper panels of Fig. 2 show the residual anisotropy produced by three BV models. The background is open ($\Omega_0 = 0.2$), the wall width is $d_w = 5h^{-1}\ Mpc$ in all the cases, and the values of the amplitude $(\frac{\Delta\rho}{\rho})_{max}$ are 2, 4 and 6. The present energy density contrasts of these models are presented in the upper panel of Fig. 1. The initial values of the free parameters are given in Table 1. In the upper left (right) panel of Fig. 2, the void is centred at $z = 0.0052$ ($z = 2.42$). The first of these redshifts corresponds to the location of the true BV and the second one to the position leading to the maximum anisotropy (see below). As it is observed in the plot, the greater $(\frac{\Delta\rho}{\rho})_{max}$, the greater the amplitude of δ_R. In the upper left (right) panel, the maximum amplitude of the residual anisotropy is $\delta_R \sim 8 \times 10^{-7}$ ($\delta_R \sim 4.5 \times 10^{-6}$); this value is obtained in the case $(\frac{\Delta\rho}{\rho})_{max} = 6$. For the model $d_w = 5h^{-1}\ Mpc$, $(\frac{\Delta\rho}{\rho})_{max} = 4$, the residual anisotropies are $\delta_R \sim 4 \times 10^{-7}$ (left) and $\delta_R \sim 2.3 \times 10^{-6}$ (right).

The bottom panels of Fig. 2 also display the residual anisotropy produced by three BV models. The background is the same as in the upper panels, but the realizations are different. The wall widths, are $3h^{-1}\ Mpc$, $5h^{-1}\ Mpc$ and $7h^{-1}\ Mpc$ and the amplitude is $(\frac{\Delta\rho}{\rho})_{max} = 4$ in all the cases. The present energy density contrasts of these models are given in the intermediate panel of Fig. 1 and the initial conditions can be found in Table 1. The redshifts of the void centres are the same as in the top panels: $z = 0.052$ (left) and $z = 2.42$ (right). In the bottom left (right) panel, the

maximum amplitude of the residual anisotropy is $\delta_{R} \sim 6.8 \times 10^{-7}$ ($\delta_{R} \sim 3.8 \times 10^{-6}$). These values correspond to the maximum wall width $d_w = 7h^{-1}\ Mpc$. The greater d_w, the greater the amplitude of δ_{R}.

All the cases of the left panels of Fig. 2 correspond to the same backgrounds and locations and the central underdense regions have the same structure; hence, the differences between the anisotropies of two of these cases are due to the wall. The same can be stated for the cases of the right panels. In the cases corresponding to the continuous and dashed lines, the anisotropy produced by the wall dominates the total effect.

The upper panel of Fig. 3 shows the residual anisotropy produced by the model $\Omega_0 = 0.2$, $(\frac{\Delta\rho}{\rho})_{max} = 4$, and $d_w = 5h^{-1}\ Mpc$. Each curve corresponds to a location of the void. The redshift defining this location is given inside the panel. This model is also considered in Fig. 2. As it is shown in this panel, the amplitude of the residual anisotropy is an increasing function of the redshift z –defining the location of the void– from $z = 0.052$ to $z \simeq 2.42$, while it becomes a decreasing function for $z > 2.42$. The maximum amplitude is 2.36×10^{-6}, it is is found at $z \simeq 2.42$. As it is pointed out below, this behavior is not observed in the case of flat models.

Fig. 4 shows the density profiles of the three realizations described in the top panel of Fig. 1, for $z = 2.42$ and $\Omega_0 = 0.2$. As it can be seen in Fig. 4, these structures were evolving in the mildly nonlinear regime when they produced the maximum anisotropy. The amplitude of the density contrast inside the underdensity

is -0.59 in all the cases. Inside the wall, this amplitude takes on the values 0.48, 0.69 and 0.82 for the amplitudes 2, 4 and 6, respectively; hence, the standard Eulerian linear approach does not apply.

4.2 Flat Universe, $\Omega_0 = 1$

For $\Omega_0 = 1$, the residual anisotropy corresponding to the realization $(\frac{\Delta\rho}{\rho})_{max} = 4$, $d_w = 5h^{-1}\ Mpc$ is shown in the intermediate panel of Fig. 3. The void centre is located at the redshifts displayed inside the panel. The initial conditions are given in Table 2. For a flat background, the amplitude of the anisotropy produced by the chosen BV realization (the same as in the top panel of Fig. 3) is $\sim -3.2 \times 10^{-7}$ in the case $z = 0.052$. The modulus of this amplitude decreases as z increases from $z = 0.052$ to $z \simeq 2.42$ and it is an slowly increasing function of z for $z > 2.42$; hence, at redshifts between 1 and 10, the value of this modulus is much smaller than the amplitude of the residual anisotropy corresponding to the open case (top panel of Fig. 3). At $z = 2.42$, the ratio between this amplitude and the mentioned modulus is ~ 8; therefore, we can state that, at low redshifts, the anisotropies corresponding to the open case are much greater than those of the flat case.

In the intermediate panel of Fig. 3, it can be seen that the wall produces a local effect. When the structure is located at $z = 0.052$, this effect appears between $\psi = 8°$ and $\psi = 13°$. As the redshift increases, the effect appears at smaller angles. In any case, the angular position of the feature coincides with that of the sharped wall. The

photons coming along these directions cross a great part of the wall. The accuracy of our codes allows us to obtain these small features.

The sign of $\delta_{_R}(\psi = 0)$ is positive for $\Omega_0 = 0.2$ and negative for $\Omega_0 = 1$ (see the upper and intermediate panels of Fig. 3). In the absence of walls (Arnau et al. 1993) as well as in the case of small compensating walls (Panek 1992), the sign of $\delta_{_R}(\psi = 0)$ is negative for both Ω_0 values; therefore the sign change only appears in the case of overcompensated voids.

4.3 Comparisons with previous calculations

Panek (1992) studied four void realizations evolving in a flat background. The model (c) of Panek's paper is a BV model having the following features: $\Omega_0 = 1$, $(\frac{\Delta\rho}{\rho})_v \sim -1$, $R_v \sim 30h^{-1}\ Mpc$, $(\frac{\Delta\rho}{\rho})_{max} \sim 2.5$ and $d_w \sim 2h^{-1}\ Mpc$. Our code –based on the gradient method– has been used in order to find the initial conditions corresponding to this model. The values of ε_1, ε_2, R_{x1} and R_{x2} are given in Table 2 (second row). The present density contrast of this model is displayed in the bottom panel of Fig. 1. It has been verified that the wall compensates the central underdensity at $R_c = 51.6h^{-1}\ Mpc$. As in Panek's paper, the void centre is placed at $100h^{-1}\ Mpc$ from the observer in order to compute anisotropies. The residual anisotropy produced by this model is plotted in the bottom panel of Fig. 3. This panel and the bottom panel of Fig. 1 are to be compared with Figs. 6 and 1 of Panek's paper, respectively. These panels have a special format –different from that of the remaining ones– in order to

facilitate comparisons with Panek's Figures (Panek 1992). These comparisons clearly show that our codes –based on the TBS and Eq. (1) and (2)– have let to a BV model very similar to that of Panek (1992); accordingly, the residual anisotropy appears to be very similar to that predicted by this author in his case (c). These results simultaneously test our codes and those used by Panek (1992).

Thompson & Vishniac (1987) and Martínez-Gonzalez & Sanz (1990) predicted BV anisotropies of a few times $\sim 10^{-7}$ for Boötes-like objects located at $z \sim 0.05$ in any admissible background and similar anisotropies for other redshifts in a flat universe. These authors used the Swiss-Cheese model. In the case of small compensating walls (bottom panel of Fig. 3) and in the absence of walls (Arnau et al. 1993), our results essentially agree with these previous estimates; however, under the following assumptions: (1) overcompensating walls with the features suggested by the observational data, (2) an open universe with $\Omega_0 = 0.2$, and (3) low redshifts ranging in the interval (1,10), previous predictions are magnified by a factor ~ 10.

5 Conclusions and discussion

Equation (1) defines a good parametrization of the initial density profiles in the case of voids with sharped walls. Our code based on the gradient method –plus Eqs (1) and (2)– gives the initial conditions leading to any BV model.

As a result of the fact that the void walls have been modeled taking into account the observational evidences, the compensation of the central underdensity takes place

at scales larger than that of a single void. Various voids contribute to this compensation.

The anisotropy produced by a Boötes-like void strongly depends on the wall structure, the density parameter and the location of the symmetry centre. According to previous estimates, which are confirmed in this paper, the anisotropy produced by compensated voids evolving in a flat universe has an amplitude of a few times 10^{-7}; however, for $\Omega_0 = 0.2$ and locations between $z = 1$ and $z = 10$, the overcompensated voids suggested by the observations produce anisotropies of a few times 10^{-6} on scales of a few degrees. A question is relevant: What is the effect produced by a distribution of voids in an open universe?. In the flat case $\Omega_0 = 1$, the anisotropies corresponding to the same range of redshifts are much smaller. The value of the density parameter is of crucial importance. In the case of overcompensating walls, the sign of the effect towards the central region of the void is positive (negative) for open (flat) universes. If this effect is detected in future in the case of a single observable structure, results could be used in order to constraint the density parameter; nevertheless, it should be pointed out that such a detection is not easy, in particular, in the flat case, where the resulting anisotropy is very small.

For the above interval of redshifts $(1, 10)$ and $\Omega_0 = 0.2$, the present distances from the void centre to the observer range from $\sim 2000h^{-1}\ Mpc$ to $\sim 5900h^{-1}\ Mpc$. There are many voids located between these distances; nevertheless, only some rare voids would be Boötes-like voids (or greater) producing anisotropies of a few times 10^{-6}.

Given two observation angles ψ_1 and ψ_2, the number of big voids n_1 and n_2 crossed by the photons traveling along the chosen directions can be different. For $\mid n_1 - n_2 \mid > 1$, the relative temperature difference corresponding to ψ_1 and ψ_2 would be near 10^{-5}. This possibility cannot be rejected *a priori*. It must be either rejected or accepted after quantitative calculations. The feasibility of the condition $\mid n_1 - n_2 \mid > 1$ depends on the abundance of big voids. Since the anisotropy –on scales of a few degrees– observed in experiments as COBE (Smoot et al. 1992) and Tenerife (Watson et al 1992) is near 10^{-5}, the contribution of big voids at low redshifts could be important. In the flat case, this contribution is expected to be too small. In any case, it would appear superimposed to the primary anisotropy produced near the last scattering surface in the linear regime.

Similar results were obtained in the case of Great Attractor-like objects (Arnau, Fullana & Sáez 1994). For $\Omega_0 < 0.4$ and $2 < Z < 30$, these structures produce anisotropies of the order of 10^{-5} on scales of a few degrees. In both cases, either the universe is open enough or the anisotropy is negligible. Results about Great Attractor-like object enhance the interest of the above question, which should be rewritten as follows: What is the anisotropy produced by a distribution of voids and great overdensities in an open universe?.

Although a model of overcompensated isolated voids based on the TBS is currently competitive, it has some important limitations related to the spherical symmetry. Even if the central underdense region is quasispherical, the true wall is not regular

and the motion of the matter contained in this part of the structure is not strictly radial. There are clusters and structures in the walls, which produce local peculiar motions tangent to the wall. These motions would also produce anisotropy (Tuluie & Laguna 1995). The anisotropy produced by the substructures of the walls are expected to be important on angular scales smaller than a few degrees and, consequently, the estimates of this paper should be admissible.

ACKNOWLEDGMENTS

This work has been supported by the project GV-2207/94. The numerical computations have been carried out in the Computational Center of the " Universitat de València ". One of us, M.J.F., gives thanks to the "Conselleria de Cultura, Educació i Ciència de la Generalitat Valenciana" for a fellowship.

References

Anninos, P., Matzner, R.A., Tuluie, R. & Centrella, J. 1991, ApJ, 382, 71

Arnau, J.V., Fullana, M.J., Monreal, L. & Sáez, D. 1993, ApJ, 402, 359

Arnau, J.V., Fullana, M.J. & Sáez, D. 1994, MNRAS, 268, L17

Bondi, H. 1947, MNRAS, 107, 410

Bouchet, F.R., Juszkiewicz, R., Colombi, S. & Pellat, R., 1992, 394, L5

Davis, M., Huchra, J., Latham, D.W. & Tonry, J., 1982, ApJ, 253, 423

de Lapparent, V., Geller, M.J. & Huchra, J.P. 1986, ApJ, 302, L1

Dey, A., Strauss, M.A., & Huchra, J., 1990, ApJ, 99, 463

Hellaby, C. & Lake, K. 1985, ApJ, 290, 381

Kirshner, R.P., Oemler, A.Jr., Schechter, P.L. & Shectman, S.A. 1981, ApJ, 248, L57

Martínez-González, E., & Sanz, J.L. 1990, MNRAS, 247, 473

Martínez-González, E., Sanz, J.L., & Silk, J., 1990, ApJ, 355, L5

Martínez-González, E., Sanz, J.L., & Silk, J., 1992, Phys. rev., 46D, 4193

Martínez-González, E., Sanz, J.L., & Silk, J., 1994, ApJ, 436, 1

Panek, M. 1992, ApJ, 388, 225

Peebles, P.J.E., 1980, The Large Scale Structure of the Universe, Princeton Univ. Press, Princeton, NJ

Quilis, V., Ibáñez, J.M., & Sáez, D., 1995, MNRAS, in press

Rees, M., & Sciama, D.W. 1968, Nature, 217, 511

Rood, H.J., 1988, Ann. Rev. Astron. Astrophys., 26, 245

Sáez, D., Arnau, J.V. & Fullana, M.J. 1993, MNRAS, 263, 681

Smoot, G.F. et al., 1992, ApJ, 396, L1

Thompson, K.L. & Vishniac, E.T. 1987, ApJ, 313, 517

Tolman, R.C. 1934, Proc. Natl. Acad. Sci., 20, 169

Tuluie, R., & Laguna, P., 1995, ApJ, 445, L73

Vettolani, G., de Souza, R.E., Marano, B., & Chincarini, G., 1985, Astron. Astrophys., 144, 506

Watson, R.A., Gutierrez de la Cruz, R.D., Davies, R.D., Lasenby, A.N., Rebolo, R., Beckman J.E., & Hancock S., 1992, Nat, 357, 660

Figure Captions

Fig. 1. Present density contrast $\Delta\rho/\rho(t_0)$ as a function of the present radial distance R_0 in units of h^{-1} Mpc. Upper panel corresponds to three BV realizations with the same wall width $d_w = 5h^{-1}$ Mpc and three different amplitudes displayed inside the panel. The BV realizations of the intermediate panel correspond to the fixed amplitude $(\frac{\Delta\rho}{\rho})_{max} = 4$ and the wall widths are shown inside the panel in units of h^{-1} Mpc. Bottom panel corresponds to $(\frac{\Delta\rho}{\rho})_{max} = 2.5$, $d_w = 2h^{-1}$ Mpc.

Fig. 2. Left panels show the residual anisotropy $\delta_R \times 10^7$ as a function of the observation angle ψ (in degrees) for several BV realizations placed at $z = 0.052$. The density parameter is $\Omega_0 = 0.2$. Upper (bottom) left panel corresponds to the same BV realizations as in the upper (intermediate) panel of Fig. 1. Right panels display the quantity $\delta_R \times 10^6$ for the same models as in the left panels. Void centres are located at $z = 2.42$.

Fig. 3. Same as Fig. 2. Top panel corresponds to the realization $(\frac{\Delta\rho}{\rho})_{max} = 4$, $d_w = 5h^{-1}$ Mpc evolving in an open universe with $\Omega_0 = 0.2$. This realization is placed at the redshifts displayed inside the panel. In the intermediate panel the realization and the redshifts are identical to those of the top panel, but the background is flat. The bottom panel corresponds to the energy density profile of the bottom panel of Fig. 1. The background is flat.

Fig. 4. Density contrast $\Delta\rho/\rho$ as a function of the radial distance R at redshift 2.42. R is given in units of h^{-1} Mpc. The three BV realizations have the same wall width $d_w = 5h^{-1}$ Mpc and three different amplitudes displayed inside the panel. The density parameter is $\Omega_0 = 0.2$.

Table 1. BV models. $\Omega_0 = 0.2$.

$(\frac{\Delta\rho}{\rho})_{max}$	d_w $(h^{-1}Mpc)$	$\varepsilon_1 \times 10^3$	$\varepsilon_2 \times 10^2$	$R_{x1} \times 10^2$ $(h^{-1}Mpc)$	$R_{x2} \times 10^2$ $(h^{-1}Mpc)$	R_c $(h^{-1}Mpc)$
2.	5.	34.22	-4.29	2.60	2.32	35.9
4.	5.	5.70	-1.44	3.63	2.09	32.7
6.	5.	4.91	-1.36	4.31	2.06	32.4
4.	3.	23.44	-3.21	2.70	2.32	33.3
4.	7.	4.63	-1.33	4.21	2.05	32.8

Table 2. BV models. $\Omega_0 = 1$.

$(\frac{\Delta\rho}{\rho})_{max}$	d_w $(h^{-1}Mpc)$	$\varepsilon_1 \times 10^3$	$\varepsilon_2 \times 10^3$	$R_{x1} \times 10^2$ $(h^{-1}Mpc)$	$R_{x2} \times 10^2$ $(h^{-1}Mpc)$	R_c $(h^{-1}Mpc)$
4.	5.	1.43	-3.63	3.65	2.08	32.7
2.5	2.	0.14	-12.06	6.53	0.99	51.6

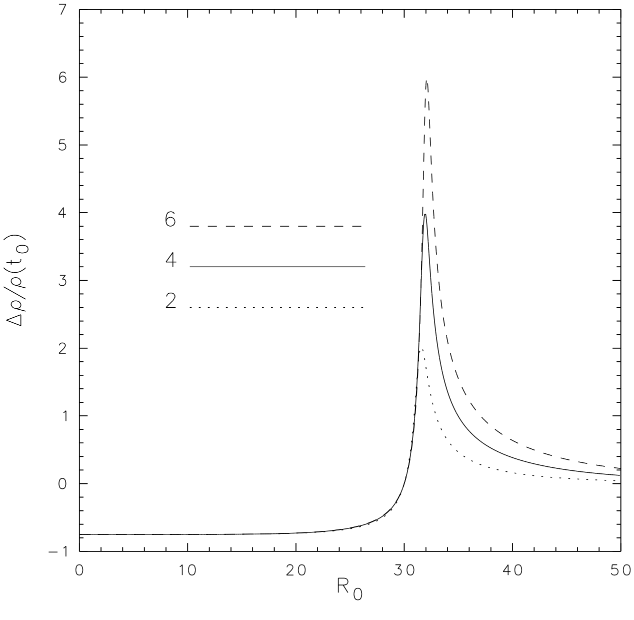

6
4
2
Δρ/ρ(t0)
R0

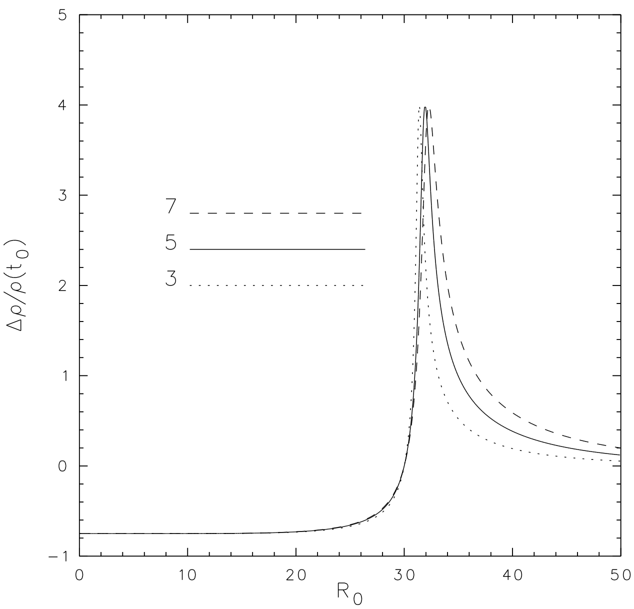

7
5
3
Δρ/ρ(t0)
R0

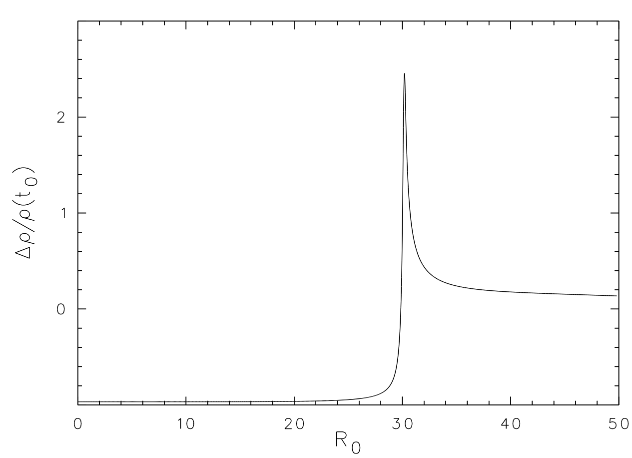

Δρ/ρ(t0)
R0

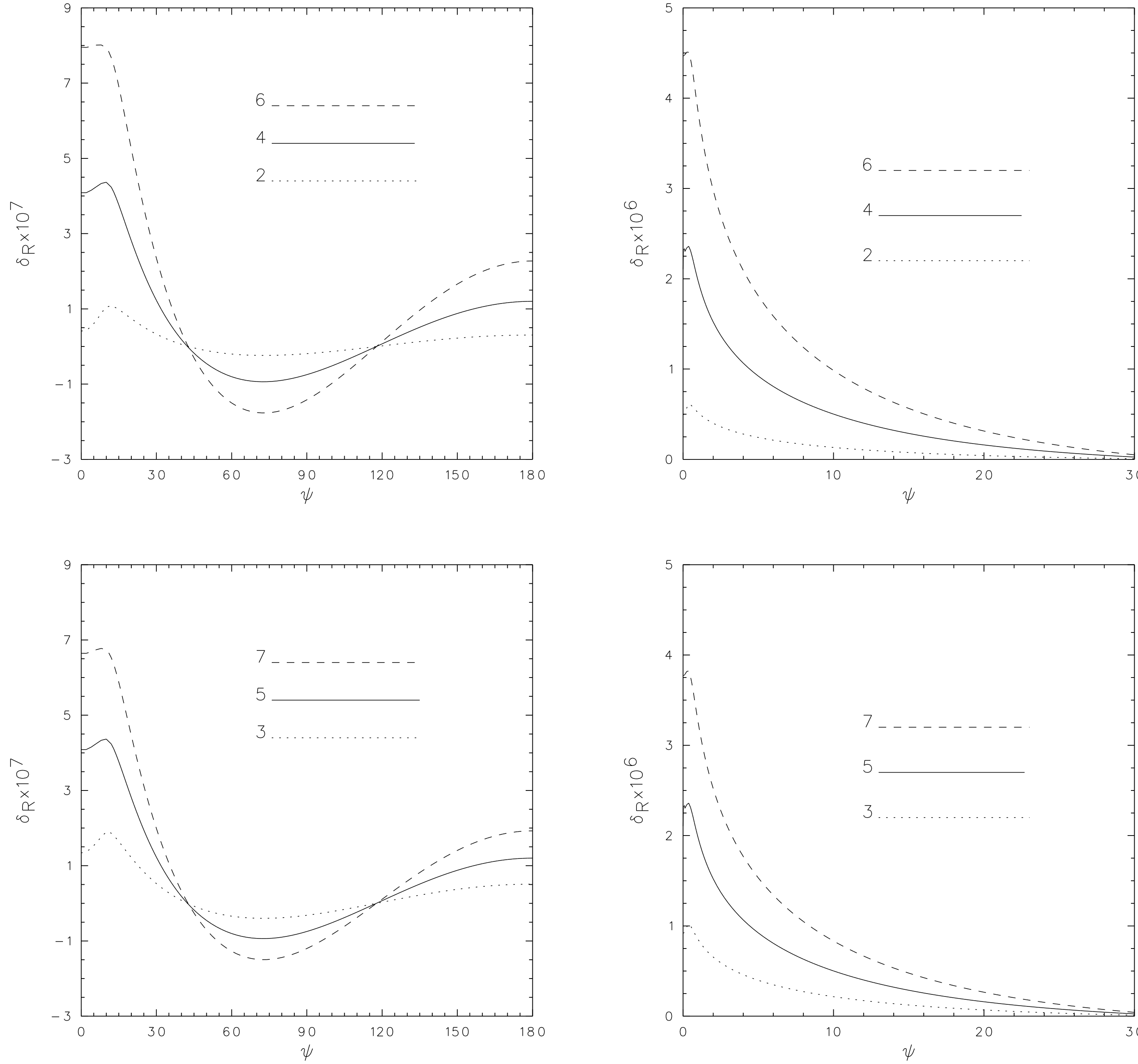

δR×10^7
ψ
6
4
2
δR×10^6
ψ
6
4
2
δR×10^7
ψ
7
5
3
δR×10^6
ψ
7
5
3

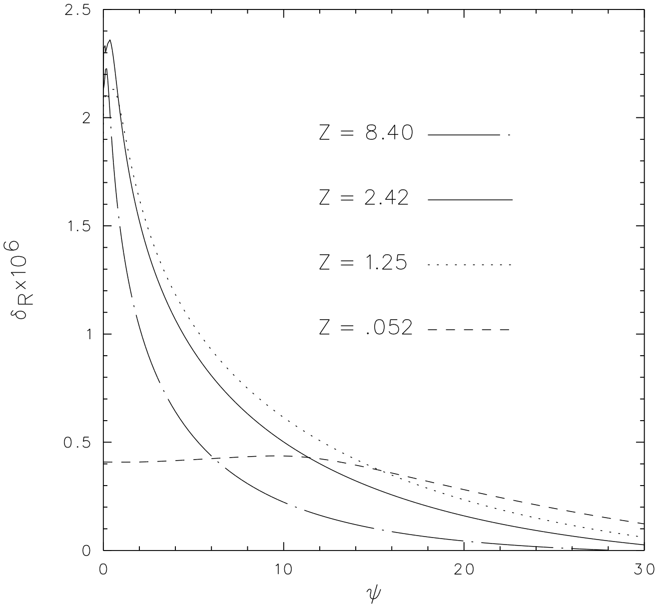

Z = 8.40
Z = 2.42
Z = 1.25
Z = .052
δRx10^6
ψ

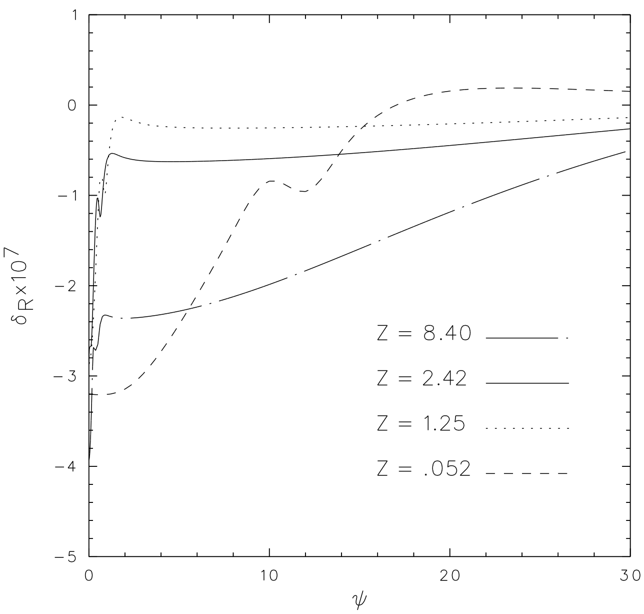

Z = 8.40
Z = 2.42
Z = 1.25
Z = .052
δRx10^7
ψ

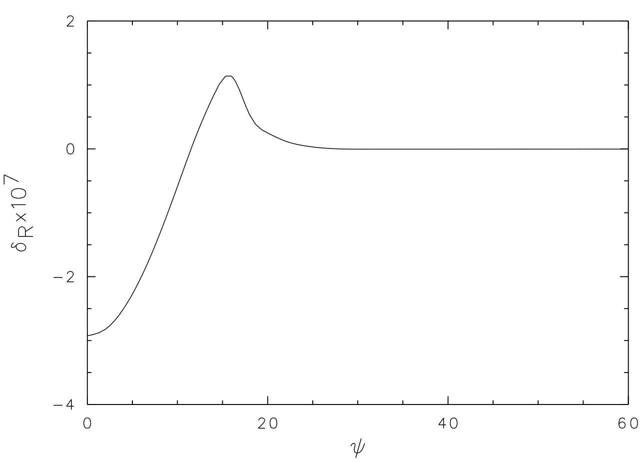

δRx10^7
ψ

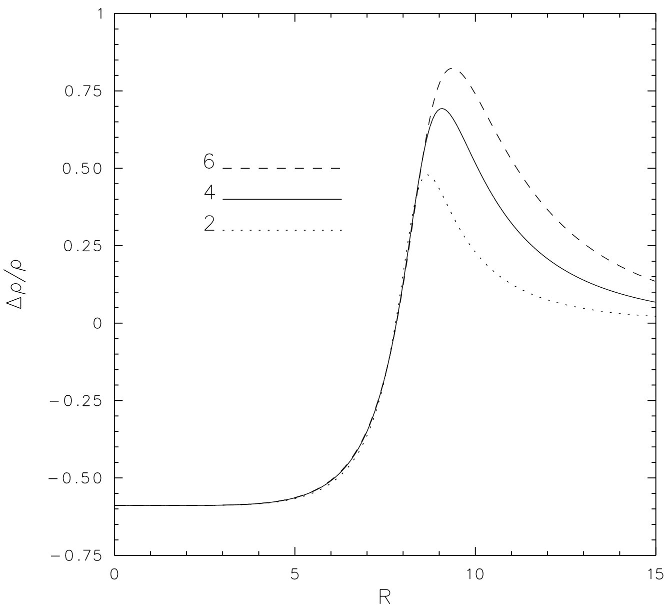

1
0.75
0.50
0.25
0
−0.25
−0.50
−0.75
0
5
10
15
R
Δρ/ρ
6
4
2